



HAL
open science

Enantioseparation of fluorinated 3-arylthio-4,4'-bipyridines: Insights into chalcogen and π -hole bonds in high-performance liquid chromatography

Paola Peluso, Carlo Gatti, Alessandro Dessì, Roberto Dallochio, Robin Weiss, Emmanuel Aubert, Patrick Pale, Sergio Cossu, Victor Mamane

► To cite this version:

Paola Peluso, Carlo Gatti, Alessandro Dessì, Roberto Dallochio, Robin Weiss, et al.. Enantioseparation of fluorinated 3-arylthio-4,4'-bipyridines: Insights into chalcogen and π -hole bonds in high-performance liquid chromatography. *Journal of Chromatography A*, 2018, 1567, pp.119-129. 10.1016/j.chroma.2018.06.060 . hal-02106490

HAL Id: hal-02106490

<https://hal.science/hal-02106490>

Submitted on 6 Jan 2022

HAL is a multi-disciplinary open access archive for the deposit and dissemination of scientific research documents, whether they are published or not. The documents may come from teaching and research institutions in France or abroad, or from public or private research centers.

L'archive ouverte pluridisciplinaire **HAL**, est destinée au dépôt et à la diffusion de documents scientifiques de niveau recherche, publiés ou non, émanant des établissements d'enseignement et de recherche français ou étrangers, des laboratoires publics ou privés.

Enantioseparation of fluorinated 3-(aryl)thio-4,4'-bipyridines: insights into chalcogen and π -hole bonds in high-performance liquid chromatography

Paola Peluso,^{a,*} Carlo Gatti,^{b,c} Alessandro Dessì,^a Roberto Dallochio,^a Robin Weiss,^d Emmanuel Aubert,^e Patrick Pale,^d Sergio Cossu^f and Victor Mamane^{d,*}

^a Istituto di Chimica Biomolecolare ICB, CNR, Sede secondaria di Sassari, Traversa La Crucca 3, Regione Balduca, 07100 Li Punti - Sassari, Italy

^b CNR-ISTM, Istituto di Scienze e Tecnologie Molecolari, via C. Golgi 19, 20133 Milano, Italy

^c Istituto Lombardo Accademia di Scienze e Lettere, via Brera 28, 20121 Milano

^d Institut de Chimie de Strasbourg, UMR CNR 7177, Equipe LASYROC, 1 rue Blaise Pascal, 67008 Strasbourg Cedex, France

^e Cristallographie, Résonance Magnétique et Modélisations (CRM2), UMR CNRS 7036, Université de Lorraine, Bd des Aiguillettes, 54506 Vandoeuvre-les-Nancy, France

^f Dipartimento di Scienze Molecolari e Nanosistemi DSMN, Università Ca' Foscari di Venezia, Via Torino 155, 30172 Mestre Venezia, Italy

* Corresponding author. E-mail address: p.peluso@icb.cnr.it. Tel.: +39 079 2841218.

* Additional corresponding author. E-mail address: vmamane@unistra.fr. Tel.: +33 368 851612.

ABSTRACT

A chalcogen bond (ChB) is a σ -hole-based noncovalent interaction between a Lewis base and an electrophilic element of Group VI (O, S, Se, Te), which behaves as a Lewis acid. Recently, we demonstrated that halogen bond, the more familiar σ -hole-based interaction, is able to promote the enantioseparation of chiral compounds in HPLC environment. On this basis, an investigation to detect ChBs, functioning as stereoselective secondary interactions for HPLC enantioseparations, was started off and the results of this study are described herein. Our investigation also focused on the impact of the perfluorinated aromatic ring as a π -hole donor recognition site. For these purposes, seven atropisomeric fluorinated 3-(aryl)thio-4,4'-bipyridines were designed, synthesized and used as potential ChB donors (ChBDs) with two cellulose-based chiral stationary phases (CSPs) containing carbonyl groups as ChB

28 acceptors (ChBAs). In addition, one and two analogues lacking fluorine and sulphur, respectively, were
29 prepared as terms of comparison. The design of the test analytes was computationally guided. In this
30 regard, electrostatic potentials (EPs) associated with σ - and π -holes were computed and the atomic
31 contributions to the sulphur EP maxima were derived using a molecular space partitioning in terms of
32 Bader's atomic basins. This procedure is akin to the Bader-Gatti electron density source function (SF)
33 decomposition, yet suitably extended to the EP field. For five 3-substituted-4,4'-bipyridines,
34 thermodynamic parameters were derived from van't Hoff plots. Finally, the use of molecular dynamic
35 (MD) simulation to model ChB in cellulose-analyte complexes was explored. Evidences that σ -hole and
36 π -hole interactions can jointly drive HPLC enantioseparations through recognition sites generated by
37 local electron depletion emerged from both experimental results and theoretical data.

38

39

40

41

42 *Keywords:* Bipyridines; Chalcogen bond; Electrostatic potential surfaces; Molecular dynamic;
43 Polysaccharide-based chiral stationary phases; Source function

44

45 **1. Introduction**

46 The enantioseparation of chiral compounds through the so-called direct approach is an important
47 matter in several fields of chemistry, biochemistry and life science [1,2]. Easy in its essence, the direct
48 approach is based on the transformation of enantiomers into transient diastereomeric complexes in a
49 chiral environment generated by a chiral selector. Nevertheless, understanding the recognition pattern
50 occurring in these processes keeps on being a demanding issue in separation science [3]. Indeed, along
51 with strong long-range interactions involved in the non-stereoselective binding, diverse short-range
52 directional interactions based on the complementarity of selector and analyte (electrostatic fit), including
53 hydrogen bonds, π - π , dipole-dipole, and van der Waals interactions [4], are able to promote the
54 enantioseparation. Moreover, steric and hydrophobic factors can also play a role [1,5].

55 Currently, σ -hole bonds involving atoms of Groups IV–VII are also considered as important
56 directional noncovalent interactions and applied in several fields [6,7]. A σ -hole indicates the region of
57 positive electrostatic potential (EP) found on an anti-bonding σ^* orbital, located along the elongation of
58 a covalent bond. Typically, a σ -hole bond can be written as EWG– $D_\sigma \cdots A$ (B_L), where D_σ is the donor
59 atom, which serves as a Lewis acid, and A is the acceptor moiety with properties as a Lewis base (B_L).
60 The electron-withdrawing group (EWG) covalently attached to the D_σ redistributes the electron density
61 on the D_σ itself (anisotropy), forming electron-deficient σ -holes which, consequently, act as a Lewis
62 acid. In general, the depth of a σ -hole increases as the polarizability of D_σ [8].

63 Recently, our groups discovered that halogen bonds (XBs), belonging to the family of the σ -hole
64 bonds, can drive HPLC enantioseparations of halogenated analytes (XB donors) [9] by using cellulose
65 tris(3,5-dimethylphenylcarbamate) (CDMPC) as a chiral selector (XB acceptor) [10,11], enlarging the
66 range of interactions which are active in HPLC environment. Later, envisaging for the polysaccharide
67 derivatives a novel function other than resolution of racemic mixture [12], we showed that HPLC and

68 polysaccharide-based chiral stationary phases (CSPs) can be used as technical and molecular tools,
69 respectively, for detection of stereoselective XBs [13] (Fig. 1).

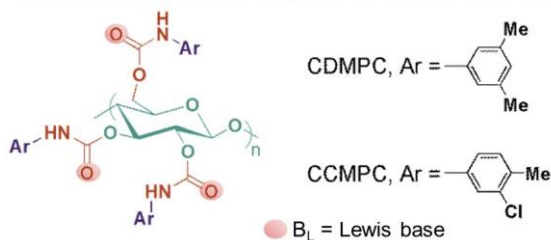
A halogen bond



Hal = Cl, Br, I

EWG = electron-withdrawing group

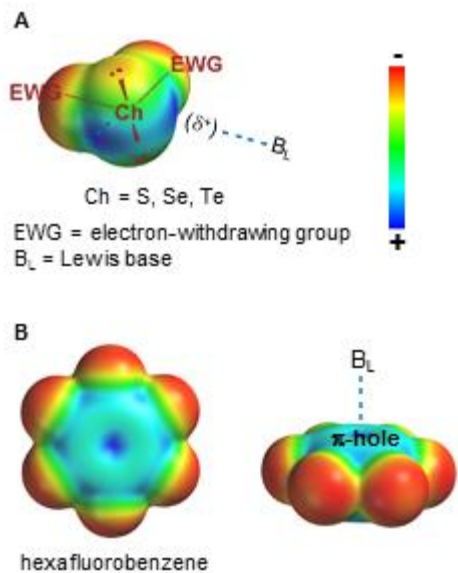
B polysaccharide-based polymers as halogen bond acceptors



70

71 **Fig. 1.** Description of halogen bond (XB) (A) and polysaccharide-based polymers as XB acceptors (B).

72 Less studied than XBs as σ -hole interactions, in the last years chalcogen bonds (ChBs) have found
73 application in materials and crystal engineering [14], self-assembly processes [15], anion binding and
74 transportation [16,17], and catalysis [18,19].



75

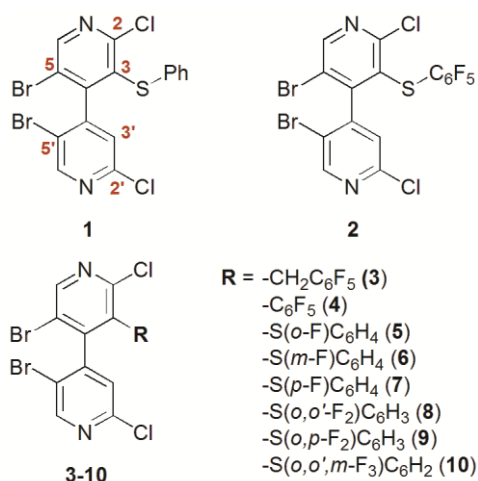
76 **Fig. 2.** General description of chalcogen (ChB) (A) and π -hole bond (B).

77 The general scheme of the ChB is depicted in Figure 2A, in which Ch is an electrophilic chalcogen
78 atom (Group VI: O, S, Se, Te) and B_L is a donor site. Analogously to the XB, the main characteristics of

79 ChB are directionality and tunability. Indeed, two regions of positive EP are localized on the outer part
80 of the Ch atom, opposite to each EWG (typical EWG–Ch··· B_L bond angles are close to 180°), and the
81 strength of the ChB can be tuned by varying Ch atom, EWG and B_L [14].

82 Conceptually analogous to the σ -hole bond, a π -hole bond is a noncovalent interaction which
83 involves an unpopulated π^* orbital (π -hole), as a donor, and a B_L as acceptor (anion or lone-pair). A
84 typical π -hole is located perpendicular to the molecular framework of perfluorinated aromatic rings (Fig.
85 2B) [6,20].

86 Further to our recent results on the XB interactions, in this paper we describe the results of a study
87 aiming to detect, in HPLC environment, other interactions involving regions of electron depletion as
88 recognition sites at both chiral and achiral level. For this purpose, atropisomeric 4,4'-bipyridines **1**, **2** and
89 **5-10** (Fig. 3) were designed as potential ChB donors (ChBDs) and synthesized in their racemic form
90 through focused procedures. In addition, perfluorinated compounds **3** and **4**, lacking sulphur at position
91 3, were designed and prepared as terms of comparison with the aim to evaluate the impact of the
92 pentafluorophenyl-centred π -hole on the enantioseparation.



93
94 **Fig. 3.** Structures of the 5,5'-dibromo-2,2-dichloro-3-substituted-4,4'-bipyridines **1-10**.

95 For all compounds, EPs were computed [21], and atomic contributions to the EPs maxima of sulphur
96 in **1-5**, associated to ChBs, were derived using a molecular space partitioning in terms of Bader's atomic

97 basins [22]. This procedure is akin to the Bader-Gatti electron density source function (SF) approach
98 [23,24], suitably extended to the EP field [25,26].

99 The chromatographic behaviour of compounds **1-10** was evaluated on cellulose-based CSPs upon
100 structural variations of selectors, analytes and mobile phase (MP) polarity. Our previous studies proved
101 the suitability of polysaccharide polymers as probes to detect stereoselective σ -hole interactions (Fig.
102 1B). Then, a study at variable temperature was performed to determine the thermodynamic parameters
103 associated with the enantioseparation processes. Moreover, an exploration of the potential role of
104 sulphur as a ChBD site was performed by molecular dynamic (MD) [11].

105 It is worth mentioning that studies on both stereoselective ChB and π -hole bonds are unprecedented.
106 In addition, currently, $S\cdots O=C$ contacts have attracted interest because they have proved to control
107 protein folding and likely regulate enzymatic functions [6].

108 **2. Experimental**

109 *2.1. Chemicals*

110 The names and the syntheses of compounds **1-10** together with the ^1H and ^{13}C NMR, and HRMS
111 spectra are available in the Supplementary data.

112 *2.2. Chromatography*

113 An Agilent Technologies (Waldbronn, Germany) 1100 Series HPLC system (high-pressure binary
114 gradient system equipped with a diode-array detector operating at multiple wavelengths (220, 254, 280,
115 360 nm), a programmable autosampler with a 20 μl loop, and a thermostatted column compartment) was
116 employed for both analytical and multimilligram separations. Data acquisition and analyses were carried
117 out with Agilent Technologies ChemStation Version B.04.03 chromatographic data software. The UV
118 absorbance is reported as milliabsorbance units (mAU). Lux Cellulose-1 (Phenomenex, USA), Chiralcel
119 OD (Daicel, Tokyo, Japan) (cellulose tris(3,5-dimethylphenylcarbamate); 10 μm), Lux Cellulose-2
120 (cellulose tris(3-chloro-4-methylphenylcarbamate); 5 μm , Phenomenex, USA), Chiralpak IC (cellulose

121 tris(3,5-dichlorophenylcarbamate); 5 μm) and Chiralpak IA (amylose tris(3,5-
122 dimethylphenylcarbamate); 5 μm) (Chiral Technologies Europe, Illkirch, France) were used as chiral
123 columns (250 \times 4.6 mm). HPLC grade ethanol (EtOH), *n*-hexane (Hex), *n*-heptane, methanol (MeOH),
124 and 2-propanol (IPA), were purchased from Sigma-Aldrich (Taufkirchen, Germany). The retention
125 factor (*k*) was determined as $k = (t_R - t_0)/t_0$, where t_R is the retention time for the eluted enantiomer. Dead
126 time (t_0) was measured by injection of tris-*tert*-butylbenzene (Sigma-Aldrich, Taufkirchen, Germany) as
127 a non-retained compound [27]. The separation factor (α) was calculated as $\alpha = k_2/k_1$, where k_1 and k_2 are
128 the retention factors of the first- and the second-eluted enantiomer, respectively. The resolution (R_s) was
129 determined as $2(t_{R2} - t_{R1})/(W_1 + W_2)$ where W is the basewidth of peak. Analyses were performed in
130 isocratic mode at 25°C. The flow rate (*FR*) was set at 0.8 ml/min for analytical separations. For
131 compounds **1**, **2** and **4**, the enantiomer elution order (EEO) was determined by injecting enantiomers of
132 known absolute configuration. The absolute configuration was assigned as reported in the
133 Supplementary data. The van't Hoff experiments were conducted at 10, 15, 20, 25, 30 and 35°C in a
134 thermostatted column chamber equipped with a cooling system. When the temperature was changed, the
135 column was allowed to equilibrate for 1 h before injecting the samples. Additional details on
136 determination of thermodynamic parameters are reported in Supplementary data.

137 2.3. Computational

138 Conformational search was performed through molecular mechanics, using the MMFF94 force field
139 and the Spartan '10 Version 1.1.0 (Wavefunction Inc., Irvine, CA) program [28]. Geometry optimization
140 and computation of electrostatic potentials surfaces (EPSs) and related parameters (EP extrema, maxima
141 and minima values, given in kJ/mol) were performed and graphically generated (Spartan '10 Version
142 1.1.0) employing the density functional theory (DFT) method with the B3LYP functional and the 6-
143 311G* basis set (available for elements H-Ca and Ga-Kr). Calculated EPs for 4,4'-bipyridines **1-10** are
144 available in the Supplementary data. Values of the electrostatic potential onto an isovalue electron

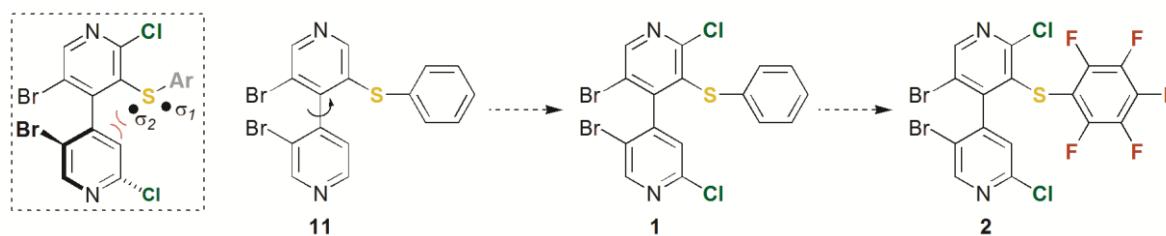
145 density surface were used as an indicator of the anisotropy of the molecular charge distribution. The
146 surface mapped values of the EP as derived from Spartan '10, used the default values of the program
147 (electron density isovalue 0.002 au, high resolution). EPS colours towards red depict negative mapped
148 potentials, while colours towards blue depict positive potentials and colours in between (orange, yellow,
149 green) depict intermediate values of the mapped potential. Min EP and max EP are the local
150 minimum(a) and the maximum(a) values of the mapped property. Search for the exact location of such
151 EP extrema was made through the Multiwfn code [29] and through its module enabling quantitative
152 analyses of molecular surfaces [30] for several isovalue surface fields and mapped properties thereon.

153 Experimental details for SF calculations and MD are available in the Supplementary data.

154 3. Results and discussion

155 3.1. Design and syntheses of analytes **1** and **2** with properties as chalcogen bond donors

156 The design of new 4,4'-bipyridines serving as ChBDs was performed by means of halogen-driven
157 structural and electronic engineering on the electron-poor 4,4'-bipyridine core with the aim to obtain
158 analytes whose chromatographic response was dependent on the σ -hole depth of sulphur. The theoretical
159 approach started from the chiral 4,4'-bipyridine core **11** (Fig. 4), where two bromines and one sulphur
160 close to the stereogenic axis serve as atropisomerism inductors and potential Ch site, respectively. Thus,
161 optimization of the system was tackled in principle by means of a two-step stereoelectronic activation of
162 the sulphur site, which consists of i) regioselective activation of **11** with chlorines, and ii) perfluorination
163 of the phenyl group of compound **1** in order to obtain **2**.



164

165 **Fig. 4.** Design of potential 4,4'-bipyridine-based ChBDs.

166 3.1.1 Electrostatic potentials and their source contribution at the sulphur electrostatic potential maxima

167 To prove the efficacy of the double activation engineered on **11** to obtain **2**, EPs of the compounds
 168 were generated by mapping the EP onto electron density isosurfaces (Supplementary data). The EP
 169 analysis is widely used for exploring and studying noncovalent interactions [31,32].

170 The distribution of the mapped EPs showed two sulphur-centred σ -holes, σ_1 and σ_2 , as two narrow
 171 separated positive regions which surround the most electron-poor sites corresponding to the max EP
 172 values on sulphur. These regions are located along the elongation of each C-S bond (Fig. 4), σ_1 (at the
 173 top of Het-S bond, Het = C₁₀H₅Br₂N₂ for **11**, and C₁₀H₃Br₂Cl₂N₂ for **1** and **2**) being more electronically
 174 activated and sterically accessible than σ_2 (at the top of S-Ar bond, Ar = C₆H₅ for **11** and **1**, and C₆F₅ for
 175 **2**) (Table 1). Indeed, in compound **2** the max EP associated to σ_1 (max EP 114.4 kJ/mol) increases
 176 (+115%) more than the max EP of σ_2 (max EP 52.0 kJ/mol) (+38.3%), relative to the corresponding EP
 177 values in **11** (σ_1 , σ_2 : 53.2, 37.6 kJ/mol).

178 **Table 1**
 179 Calculated EP^a values [kJ/mol] for compounds **1**, **2** and **11** (Spartan '10 V1.1.0, DFT, B3LYP/6-311G*).

4,4'-bipy	max EP (S) (σ_1 , σ_2)	max EP (Ar _{pyr})	min EP (N _{pyr})	max EP (Ar _F)	max EP (3-Br)	max EP (3'-Br)	max EP (2-Cl)	max EP (2'-Cl)
11	53.2, 37.6	46.3	-164.8	--	94.5	84.3	--	--
1	59.9, 52.5	73.0	-148.6	--	114.3	106.2	49.7	48.0
2	114.4, 52.0	86.1	-144.0	105.7	124.5	116.3	69.5	50.8

180 ^a EP electrostatic potential.

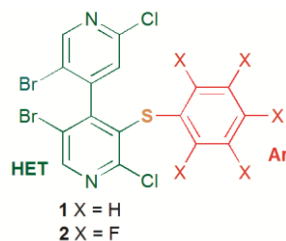
181 From the EP analysis, different effects on σ_1 and σ_2 can be assigned to the two types of activation: i)
 182 the introduction of two chlorines, at positions 2 and 2', increases the max EP value of σ_2 (**1**: max EP
 183 52.5 kJ/mol, + 39.6%) more than for σ_1 (**1**: max EP 59.9 kJ/mol, + 12.6%); ii) on the contrary, with the
 184 subsequent perfluorination, the max EP value of σ_1 increases dramatically (**2**: max EP 114.4, + 91%),
 185 whereas the max EP in σ_2 remains almost unchanged.

186 In addition, in compound **2** a positive EP (**2**: max EP 105.7 kJ/mol) on the perfluorinated aromatic
 187 ring revealed the presence of a π -hole as a potential recognition site. Moreover, in **1** and **2** the common
 188 5,5'-dibromo-2,2'-dichloro-4,4'-bipyridyl scaffold showed four halogen-centred σ -holes.

189 With the aim to examine in depth the origin of the EP on sulphur, we applied the SF [33] EP
 190 decomposition [25,26] to the sulphur-centred σ -holes in both **1** and **2**. Within this approach, each EP
 191 value may be envisaged as due to source contributions from the atoms or groups of atoms of a system.
 192 On this basis, it is possible to evaluate how the EP at the σ -hole is influenced by the remaining parts of
 193 the system and the small or large extent of such influence is just quantified by the SF. In Table 2, the EP
 194 SF decomposition in **1** and **2** at the EP maxima of sulphur σ_1 and σ_2 is reported. The values of V
 195 represent the SF contributions of the listed atomic groups, while those of ΔV express the change of such
 196 contributions on passing from **1** to **2** [$\Delta V = V(2) - V(1)$]. The sign of source is positive or negative
 197 whether the atomic (or group) source concurs or opposes to the positive potential of σ_1 and σ_2 .

198 **Table 2**

199 EP (au) SF^a decomposition in **1** and **2** at the electrostatic potential maxima of sulphur σ_1 and σ_2 on the 0.002 au electron density surface.^b



200

Atomic groups	1	2	1 \rightarrow 2
	V ^c [au]	V ^c [au]	ΔV^d [au]
	σ_1 (1.90 Å ^e ; 0.0285 au) ^f	σ_1 (1.94 Å ^e ; 0.0495 au) ^f	(0.0210) ^f
Het	-0.0041	0.0019	0.0060
All Halogen atoms	-0.0329	-0.0325	0.0004
All [C _{Ar} + H _{Ar} (F) _{Ar}]	-0.0022	-0.0184	-0.0162
S	0.0359	0.0665	0.0306
	σ_2 (1.94 Å ^e ; 0.0268 au) ^f	σ_2 (2.02 Å ^e ; 0.0272 au) ^f	(0.0004) ^f
Het	-0.0175	-0.0118	0.0057
All Halogen atoms	-0.0433	-0.0451	-0.0018
All [C _{Ar} + H _{Ar} (F) _{Ar}]	0.0038	-0.0119	-0.0157
S	0.0416	0.0515	0.0099

201 ^a EP electrostatic potential; SF source function.

202 ^b Full source function calculation data are reported in the
 203 Supplementary data

204 ^c V, SF atom/group contribution.

205 ^d $\Delta V = V(2) - V(1)$, EP atom/group contribution change on passing
 206 from **1** to **2**

207 ^e σ distance from sulphur nucleus.

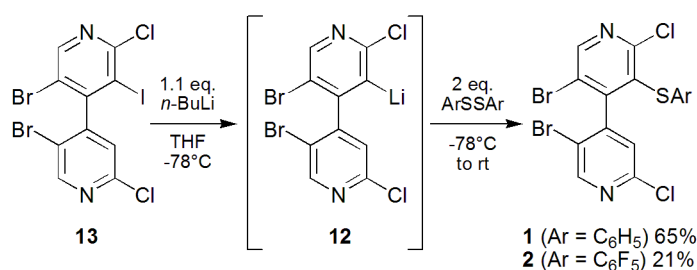
208 ^f Reference values of EP at σ_1 and σ_2 were calculated at DFT level of
 209 theory with the B3LYP functional and the 6-311G* basis set.

210 In Table 2, the sum of V(Het)+V{All [C_{Ar} + H_{Ar} (or F)_{Ar}]}+V(S) reproduces, as expected, the
 211 observed EP maxima in **1** and **2**. The V(Het) contributions include those of the halogen atoms, which

212 are also separately listed in Table 2. These latter remain almost constant, on passing from **1** to **2**, for
213 both σ_1 and σ_2 maxima ($\Delta V(\text{Het}) = 0.0004$ and -0.0018 au, respectively), while $V(\text{Het})$ similarly
214 increase for both maxima in **2** ($\Delta V(\text{Het}) = 0.0060$ and 0.0057 au, respectively). What leads to a much
215 larger σ_1 maximum upon fluorination is the almost doubling of the S atom contribution, from 0.0359 (**1**)
216 to 0.0665 au (**2**). The $\Delta V_{\text{s atom contribution}} = 0.0306$ au largely overwhelms the negative contribution of the
217 $[\text{C}_{\text{Ar}} + \text{F}_{\text{Ar}}]$ group ($\Delta V = -0.0162$ au), while for the σ_2 maximum the opposite occurs ($\Delta V_{\text{s atom contribution}} =$
218 0.0099 au; ($\Delta V_{\text{All } [\text{C}_{\text{Ar}} + \text{F}_{\text{Ar}}]} = -0.0157$ au), due to the different geometrical location of the two maxima.
219 Due to the large electron-withdrawing power of fluorine, the sulphur atom becomes more positively
220 charged upon fluorination ($q(\text{S}) = 0.122$ and $0.208 e^-$, where $q(\text{S})$ is the Bader's net charge in **1** and **2**,
221 respectively), hence more able to produce positive EP regions in **2**, relative to **1**. However, such an
222 effect is three times as big at the top of Het-S bond (σ_1) than at the top of S-Ar bond (σ_2), [$\Delta V(\text{S}) =$
223 0.0306 and 0.0099 au], owing to the much closer proximity of the former to the strong electron-
224 withdrawing F atoms. The presence of F atoms makes the C_{Ar} atoms highly electropositive ($\Delta q(\text{C})$ about
225 $0.5 e^-$), the sulphur more positively charged and polarized in a direction counter to C-F and S-F charge
226 transfer. Fluorination of the aryl ring has therefore a large enhancement effect on the σ_1 hole of sulphur
227 due to the induced large EP contribution increase from sulphur, despite the presence of F renders $V(\text{C}_{\text{Ar}}$
228 $+ \text{F})$ highly negative, relative to $V(\text{C}_{\text{Ar}} + \text{H})$ and even more so for σ_1 . In addition, geometrical
229 parameters for the two maxima on sulphur were derived from calculations (**1**, σ_1 : 1.90 \AA , Het-S- σ angle
230 xx° ; σ_2 : 1.94 \AA , Ar-S- σ angle xx°) (**2**, σ_1 : 1.94 \AA , Het-S- σ angle xx° ; σ_2 : 2.02 \AA , Ar-S- σ angle xx°).

231 3.1.2 Syntheses of 3-(aryl)thio-4,4'-bipyridines **1** and **2**

232 In practice, racemic **1** and **2** were prepared by reaction of the *in situ* generated lithio intermediate **12**
233 with 1,2-diphenyldisulfide and 1,2-bis(pentafluorophenyl)disulfide, respectively. The intermediate **12**
234 was prepared by iodine – lithium exchange performed starting from 4,4'-bipyridine **13** (Scheme 1) [34].



235

236 **Scheme 1.** Synthesis of 4,4'-bipyridines **1** and **2**.

237 Under these conditions, after addition of electrophile, **1** and **2** were obtained with 65% and 21%

238 yield, respectively (see Supplementary data for details), and enantioseparated by HPLC. Assignment of

239 absolute configuration for **1** was achieved by single crystal XRD analysis, whereas for **2**, ECD

240 spectroscopy coupled with TD-DFT calculations was used because it could not be crystallized

241 (Supplementary data).

242 Having at disposal compounds **1** and **2**, chromatographic responses strictly dependent on the

243 electronic features of the distinctive substituent at position 3 were expected.

244 3.2. Comparative enantioseparation of 3-(phenyl)thio- and 3-(pentafluorophenyl)thio-4,4'-bipyridine

245 Four chromatographic systems were generated by the combination of CDMPC with either Hex/IPA

246 90:10 (*mix A*), hex/IPA/MeOH 90:5:5 (*mix B*) or MeOH 100% (*mix C*) and cellulose tris(3-chloro-4-

247 methylphenylcarbamate) (CCMPC) with *mix A*: CDMPC/*mix A*, CCMPC/*mix A*, CDMPC/*mix B* and

248 CDMPC/*mix C*. These four systems were used in parallel, as an orthogonal HPLC protocol [13].

249 Recently, cellulose-based CSPs proved to be suitable molecular tools to study XBs in HPLC

250 environment [10]. On this basis, we envisaged that these polysaccharide-based CSPs could be used as

251 tools also for exploring other stereoselective interactions involving recognition sites generated by local

252 electron depletion, such as ChBs. Indeed, in these CSPs the glucosyl backbone determines

253 conformational chirality [35], whereas the derivatization of the native polymer allows a perpendicular

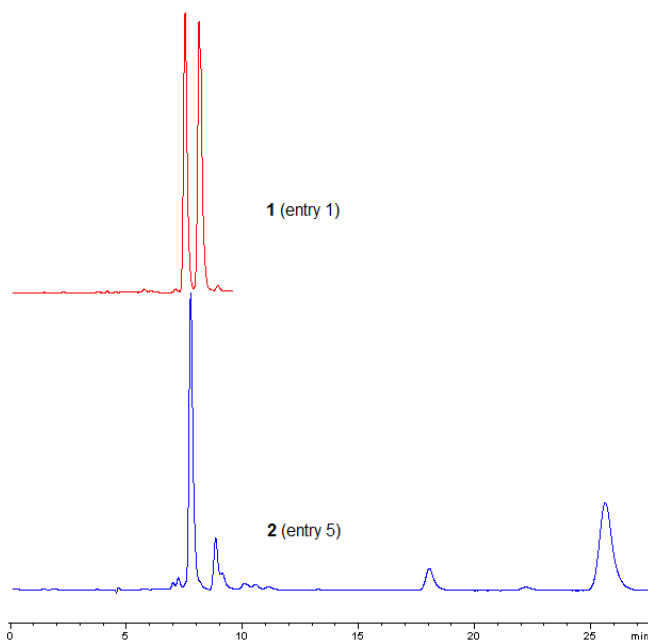
254 molecular expansion (with respect to the backbone axis) and the transfer of the chiral information to

255 generate a chiral polymeric groove which is able to host and recognize enantiomers. In this context, a

256 polar layer containing carbonyl oxygens is located inside the polymer groove, whereas a hydrophobic
257 layer containing substituted aromatic rings is located outside the polymer groove [36]. The presence of
258 methyl, as electron donating group, or chlorine, as EWG, on the aromatic ring influences the capability
259 of the carbonyl oxygens as Lewis bases [12] and, consequently, their properties as σ - / π -hole acceptors.
260 On this basis, in CDMPC the carbonyl oxygens show enhanced properties as acceptors (min $EP_{C=O}$ = -
261 170 kJ/mol). On the other hand, in CCMPC the carbonyls present reduced acceptor capability induced
262 by EW chlorine substituents (min $EP_{C=O}$ = -158 kJ/mol) [37]. Moreover, the properties of the carbonyl
263 oxygens can be triggered by tuning the MP. Indeed, hex/IPA-containing normal phase (NP) elution
264 conditions (such as *mix A*) has proved to assist interactions involving the polar layer. On the contrary,
265 MeOH-containing MPs (*mix B* and *C*) was found to destabilize σ -hole bonds forming hydrogen bonds
266 with the polar layer and promoting hydrophobic contacts [11,12].

267 On this basis, the orthogonal HPLC protocol was applied to **1** and **2** (Table 3). Retention was shown
268 to be slightly affected by the orthogonal conditions and, indeed, k_1 values for the first eluted (*M*)-
269 enantiomers range from 1.01 to 1.14 and from 0.87 to 1.26 for **1** and **2**, respectively. Analogously, both
270 k_2 and α values of **1** were scarcely influenced by any change of the chromatographic system (CSP and/or
271 MP) (entries 1-4). In these cases, hydrophobic forces seemed to control retention and selectivity. On the
272 contrary, a different behaviour was observed for compound **2** because k_2 for the second eluted (*P*)-
273 enantiomer and α values seemed to be deeply influenced by changes of analyte and CSP structures as
274 well as MP polarity (entries 5-8). On this basis, a thorough comparative analysis of chromatographic
275 data, computed electronic properties and thermodynamic parameters, derived from van't Hoff plots,
276 suggested that a stereoselective secondary interaction, strictly dependent on the (pentafluorophenyl)thio
277 substituent at the position 3 of the 4,4'-bipyridine scaffold and involving the carbamate carbonyl oxygen
278 of the CDMPC, could explain the diverse separation outcomes of **2** and **1**. In fact, taking into account the
279 effect of focused changes of donor/acceptor structures and MP, the following observations emerged:

280 **Table 3**
 281 Substitution pattern, retention and selectivity of 5,5'-dibromo-2,2'-
 282 dichloro-4,4'-bipyridines **1** and **2** on CDMPC and CCMPC under
 283 normal phase (NP) and polar organic (PO) elution modes (*FR* 0.8
 284 ml/min, *T* = 25°C).



285

entry	bipy	CSP ^a	MP ^b	<i>k</i> ₁ ^c	<i>k</i> ₂ ^c	α
1	1	CDMPC	A	1.08 (<i>M</i>)	1.25 (<i>P</i>)	1.16
2	1	CCMPC	A	1.07 (<i>M</i>)	1.19 (<i>P</i>)	1.11
3	1	CDMPC	B	1.14 (<i>M</i>)	1.29 (<i>P</i>)	1.13
4	1	CDMPC	C	1.01	1.01	1.00
5	2	CDMPC	A	1.14 (<i>M</i>)	6.12 (<i>P</i>)	5.34
6	2	CCMPC	A	0.90 (<i>M</i>)	1.18 (<i>P</i>)	1.31
7	2	CDMPC	B	1.26 (<i>M</i>)	4.61 (<i>P</i>)	3.67
8	2	CDMPC	C	0.87 (<i>M</i>)	1.80 (<i>P</i>)	2.06

286 ^a CDMPC cellulose tris(3,5-dimethylphenylcarbamate); CCMPC
 287 cellulose tris(3-chloro-4-methylphenylcarbamate).

288 ^b MP, Hex/IPA 90:10 (A); Hex/IPA/MeOH 90:5:5 (B); MeOH
 289 100% (C).

290 ^c Absolute configuration of the eluted peaks is reported.

291 i) *effect of changing analyte structure (entries 1 and 5)*. The substitution pattern of the 5,5'-dibromo-
 292 2,2'-dichloro-3-(aryl)thio-4,4'-bipyridines **1** and **2** could be correlated by changing the group at the 3-
 293 position, thus the pivotal role of σ_I depth on selectivity could be hypothesized. Indeed, the distinctive
 294 (pentafluorophenyl)thio group (max EP_S = 114.4 kJ/mol) in **2** generates a more electrophilic σ_I than the
 295 (phenyl)thio group (max EP_S = 59.9 kJ/mol) in **1**, giving, therefore, a possible explanation for the
 296 different behaviour of the two (*P*)-enantiomers (**2**: *k*₂ = 6.12, α = 5.34; **1**: *k*₂ = 1.25, α = 1.16), with a

297 79.5% decrease in the k_2 value of **1** compared to **2**, under identical elution conditions (CDMPC/*mix A*).
298 In addition, in **2** the distinctive π -hole could have an impact, as a recognition site, on the
299 enantioseparation extent, hypothesizing a π -hole interaction involving CSP carbonyl oxygen as B_L (Fig.
300 2B). On the other hand, in this compound the two chlorine-centred σ -holes at positions 2,2' showed low
301 depth and scarce capability to control selectivity [11,37]. Analogously, our previous studies on XB-
302 driven enantioseparations had showed that 5,5'-bromine-centred σ -holes, with max EP = 123.3 kJ/mol,
303 are only able to produce moderate selectivity ($\alpha = 1.47$) [11];

304 ii) *effect of changing polysaccharide structure (entries 1 vs 2 and 5 vs 6)*. By changing CDMPC to
305 CCMPC, the separation factor of **2** dramatically dropped with a 75.2% decrease, whereas the separation
306 factor of **1** showed a decrease of just 3.4%. This behaviour could be related to the reduced Lewis
307 basicity of the carbonyl groups of the CCMPC;

308 iii) *effect of changing medium polarity (entries 1 vs 3-4 and 5 vs 7-8)*. On CDMPC, the addition of
309 MeOH (*mix B* and *mix C*) enhanced MP polarity and introduced in the chromatographic system a
310 competitive electrophile. Consequently, selectivity decreased for **1** and **2** of 2.6% and 31.3% with *mix B*
311 and of 13.8% and 61.4% with *mix C*, respectively;

312 iv) *analysis of thermodynamic parameters (Table 4)*. As both retention and separation are influenced
313 by temperature, a variable temperature study was carried out between 10 and 35°C for 4,4'-bipyridines **1**
314 and **2** on the four chromatographic systems. Because the van't Hoff plots were linear in the considered
315 temperature range ($r^2 \geq 0.9958$) (Supplementary data), enthalpy and entropy values derived from the
316 plots allowed to evaluate the enthalpic and entropic contribution to enantioseparations. The derived
317 thermodynamic parameters showed that the enantiomeric separation of **1** and **2** are enthalpically driven
318 ($\Delta\Delta H < 0$ and $\Delta\Delta H < T\Delta\Delta S$) under all elution conditions. Negative ΔS indicated an increase in the order
319 of the chromatographic system as the solute moved from mobile phase to stationary phase. In particular,
320 with the system CDMPC/*mix A*, the second eluted enantiomer (*P*)-**2** showed values of enthalpy, entropy

321 and free energy ($\Delta H = -34.01 \text{ kJ}\cdot\text{mol}^{-1}$, $\Delta S^* = -98.86 \text{ J}\cdot\text{K}^{-1}\cdot\text{mol}^{-1}$, $\Delta G = -4.53 \text{ kJ}\cdot\text{mol}^{-1}$) much lower than
 322 those of (*P*)-**1** ($\Delta H = -12.27 \text{ kJ}\cdot\text{mol}^{-1}$, $\Delta S^* = -39.21 \text{ J}\cdot\text{K}^{-1}\cdot\text{mol}^{-1}$, $\Delta G = -0.58 \text{ kJ}\cdot\text{mol}^{-1}$), confirming the
 323 pivotal role of the $-\text{SC}_6\text{F}_5$ group to exert polar interactions with the CSP. It is worth mentioning that,
 324 under the same elution conditions (CDMPC/*mix A*), the thermodynamic behaviour of the couple **1/2**
 325 seemed to follow the same trend of the couple 2,2',3,3',5,5'-hexachloro- (**14**) / 2,2',3,3',5,5'-hexaiodio-
 326 4,4'-bipyridine (**15**) [13] which differ in the capability to exert σ -hole interactions in HPLC
 327 environment, iodine being privileged σ -hole donor. Indeed, $\Delta\Delta H$, $\Delta\Delta S$ and $\Delta\Delta G$ values associated to **1**
 328 ($\Delta\Delta H = -1.96 \text{ kJ}\cdot\text{mol}^{-1}$, $\Delta\Delta S = -5.32 \text{ J}\cdot\text{K}^{-1}\cdot\text{mol}^{-1}$, $\Delta\Delta G = -0.37 \text{ kJ}\cdot\text{mol}^{-1}$) are very similar to the values of
 329 the poor σ -hole bond donor **14** ($\Delta\Delta H = -1.95 \text{ kJ}\cdot\text{mol}^{-1}$, $\Delta\Delta S = -5.36 \text{ J}\cdot\text{K}^{-1}\cdot\text{mol}^{-1}$ and $\Delta\Delta G = -0.35 \text{ kJ}\cdot\text{mol}^{-1}$)
 330 ¹), whereas **2** was characterized by higher entropic stabilization ($\Delta\Delta S = -50.73 \text{ J}\cdot\text{K}^{-1}\cdot\text{mol}^{-1}$) as it occurs
 331 with the good σ -hole donor **15** [$\Delta\Delta S = -27.47 \text{ J}\cdot\text{K}^{-1}\cdot\text{mol}^{-1}$] [13].

332 **Table 4**
 333 Thermodynamic parameters calculated from the van't Hoff plots (see Supplementary data) for 2,2'-dichloro-5,5-dibromo-4,4'-bipyridines **1**
 334 and **2** on CDMPC and CCMPC under normal phase (NP) and polar organic (PO) elution modes (*FR* 0.8 ml/min).

bipy ^a	CSP ^b	MP ^c	ln <i>k</i> vs 1/T			ln α vs 1/T			
			ΔH (kJ·mol ⁻¹)	ΔS^* (J·K ⁻¹ ·mol ⁻¹)	$\Delta G_{298 \text{ K}}$ (kJ·mol ⁻¹)	$\Delta\Delta H$ (kJ·mol ⁻¹)	$\Delta\Delta S$ (J·K ⁻¹ ·mol ⁻¹)	$\Delta\Delta G_{298 \text{ K}}$ (kJ·mol ⁻¹)	
1	(<i>M</i>)	CDMPC	A	-10.31	-33.89	-0.21	-1.96	-5.32	-0.37
	(<i>P</i>)			-12.27	-39.21	-0.58			
1	(<i>M</i>)	CCMPC	A	-10.04	-33.07	-0.18	-1.59	-4.46	-0.26
	(<i>P</i>)			-11.63	-37.53	-0.44			
1	(<i>M</i>)	CDMPC	B	-9.80	-31.76	-0.33	-0.78	-1.59	-0.31
	(<i>P</i>)			-10.58	-33.35	-0.64			
1	(<i>M, P</i>)	CDMPC	C	-8.10	-27.10	-0.02	0	0	0
2	(<i>M</i>)	CDMPC	A	-14.69	-48.13	-0.34	-19.32	-50.73	-4.19
	(<i>P</i>)			-34.01	-98.86	-4.53			
2	(<i>M</i>)	CCMPC	A	-12.21	-41.88	0.28	-3.56	-9.64	-0.69
	(<i>P</i>)			-15.77	-51.52	-0.41			
2	(<i>M</i>)	CDMPC	B	-13.75	-44.22	-0.57	-14.59	-38.09	-3.23
	(<i>P</i>)			-28.34	-82.31	-3.80			
2	(<i>M</i>)	CDMPC	C	-9.99	-34.61	0.33	-8.46	-22.32	-1.80
	(<i>P</i>)			-18.45	-56.93	-1.47			

335 ^a Absolute configuration of the eluted peaks is reported.

336 ^b CDMPC cellulose tris(3,5-dimethylphenylcarbamate); CCMPC cellulose tris(3-chloro-4-methylphenylcarbamate).

337 ^c MP, Hex/IPA 90:10 (A); Hex/IPA/MeOH 90:5:5 (B); MeOH 100% (C).

338 On the other hand, the values of the thermodynamic parameters, obtained for **1** and **2** with the
 339 chromatographic system CDMPC/*mix C*, proved the higher recognition ability of the selector toward the
 340 enantiomers of **2** ($\Delta\Delta H = -8.46 \text{ kJ}\cdot\text{mol}^{-1}$, $\Delta\Delta S = -22.32 \text{ J}\cdot\text{K}^{-1}\cdot\text{mol}^{-1}$, $\Delta\Delta G = -1.80 \text{ kJ}\cdot\text{mol}^{-1}$) compared to **1**

341 (not separated). This behaviour under polar organic (PO) elution conditions could be due to higher
342 hydrophobicity and more efficient π - π stacking of **2** with respect to **1** ($\text{Log } P_{\text{partition}}$ coefficient: 6.09 (**1**) <
343 6.88 (**2**)).

344 Having identified the main features of the chromatographic behaviour of **1** and **2** with the four
345 orthogonal chromatographic systems, the enantioseparation of compounds **5-10** was explored with the
346 aim to evaluate the effect of diverse fluorine substitution patterns on the enantioseparation.

347 3.3. Enantioseparation behaviour of compounds **5-10**: effect of fluorine regiochemistry and number

348 Compounds **5-10** were designed with the aim to derive focused information on the effect of fluorine
349 regiochemistry (**5-7**) and number (**8**, **9** and **10**) from the chromatographic analysis. All this series of
350 compounds was prepared by iodine – lithium exchange performed on 4,4'-bipyridine **13** and subsequent
351 electrophilic trapping of the lithio intermediate **12** with the proper disulphide (30-71% yields), as
352 reported in Scheme 1 for **1** and **2** [34].

353 In Table 5, retention and selectivity factors observed for compounds **5-10** with the chromatographic
354 system CDMPC/mix A are reported (entries 2-7) along with the corresponding parameters of **1**, as a term
355 of comparison (entry 1).

356 **Table 5**
357 Substitution pattern, retention, selectivity, max EP at σ_I and Ar_F of 5,5-
358 dibromo-2,2'-dichloro-4,4'-bipyridines **1** and **5-10** on CDMPC under
359 normal phase (NP) elution mode (Hex/IPA 90:10, FR 0.8 ml/min, $T =$
360 25°C).

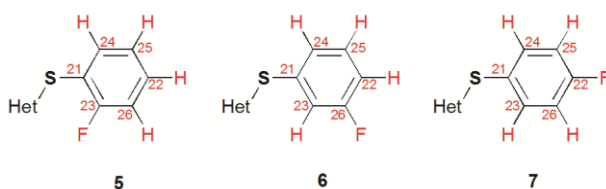
entry	bipy	fluorine pattern	max EP ^a σ_I	max EP (Ar_F)	k_1^a	k_2^a	α
1	1	--	59.9	--	1.08	1.25	1.16
2	5	<i>o</i> -F	69.8	--	1.21	1.42	1.17
3	6	<i>m</i> -F	81.4	--	1.22	1.42	1.16
4	7	<i>p</i> -F	68.6	12.0	1.20	1.30	1.08
5	8	<i>o,o</i> -F ₂	80.2	21.6	1.43	1.68	1.18
6	9	<i>o,p</i> -F ₂	79.9	25.1	1.16	1.29	1.11
7	10	<i>o,o,m</i> -F ₃	92.0	48.1	1.83	2.64	1.45

361 ^a EP electrostatic potential [kJ/mol].

362 For the mono substituted series **5-7** (entries 2-4), containing one fluorine on the phenyl ring directly
363 bonded to sulphur, retention was slightly affected by the substitution regiochemistry and, indeed, k_1

364 values for the first eluted enantiomers range from 1.20 to 1.22. Analogously, both k_2 and α values of **5**-
 365 **7** were scarcely influenced by any change of fluorine position, nevertheless selectivity was shown to
 366 decrease following the order *o*-F (**5**, $\alpha = 1.17$) > *m*-F (**6**, $\alpha = 1.16$) > *p*-F (**7**, $\alpha = 1.08$) (Fig. S7). For
 367 these compounds, a clear correlation between max EP on σ_I , max EP on Ar_F and k_2 or α was not
 368 observed. In particular, no positive value of EP related to π -hole was found for **5** and **6**, whereas a slight
 369 depletion of the electron density (max EP (Ar_F) = 12 kJ/mol) characterizes **7**.

370 **Table 6**
 371 EP(au) SF^a decomposition in **5-7** at the electrostatic potential maximum of sulphur σ_I on the 0.002 au electron density surface.^b



372

	5 σ_I (1.91 Å ^c ; 0.0323 au) ^d	6 σ_I (1.98 Å ^c ; 0.0367 au) ^d	7 σ_I (1.91 Å ^c ; 0.0322 au) ^d
Atom	V ^e	V ^e	V ^e
C ₂₁	-0.0394	-0.0308	-0.0393
C ₂₃	0.0733	0.0030	0.0023
C ₂₄	-0.0089	-0.0095	-0.0112
C ₂₆	0.0031	0.0504	0.0010
C ₂₅	-0.0006	0.0007	0.0006
C ₂₂	-0.0008	0.0008	0.0526
(C+H) _{Ar}	0.0761	0.0641	0.0621
Het	-0.0015	-0.0028	-0.0039
S	0.0442	0.0353	0.0369
F	-0.0858	-0.0589	-0.0618

373 ^a EP electrostatic potential; SF source function.

374 ^b Full source function calculation data are reported in the SI. Atoms are numbered in accordance with the source function calculation output
 375 (Supplementary data).

376 ^c σ_I distance from sulphur nucleus.

377 ^d Reference values of EP at σ_I were calculated at DFT level of theory with the B3LYP functional and the 6-311G* basis set.

378 ^e V, SF atom/group contribution. Those for the C linked to F atoms are denoted in bold.

379 Application of the SF descriptor to the sulphur-centred σ -holes in **5-7** is illustrated in Table 6. Each
 380 σ_I EP value may be expressed as a sum of contributions from the S and F atoms and from the Het and
 381 (C+H)_{Ar} groups. Data in Table 6 reveal that the single F substitution largely decreases the SF
 382 contribution of the S atom to σ_I , from 0.0665 au in **2** (Table 2) to an average value of only 0.0388 au in
 383 **5-7**, slightly larger than for the unsubstituted compound **1** (0.0359 au). Indeed the average (**5-7**) net
 384 positive charge of sulphur is 0.139 e⁻, much closer to that found in **1** (0.122) than in **2** (0.208). Increase

385 of the sulphur positive charge upon fluorination follows the substitution pattern, being larger when the
386 fluorine is closer and smaller when it is further from S (0.152, 0.140 and 0.125 for *ortho*, *meta* and *para*
387 F-substitution). Thus, the highest V(S) contribution turns out to be that of the *ortho*-F compound **5**. The
388 V(S) contribution for the *para*-F compound is, instead, surprisingly similar and even slightly larger than
389 that of the *meta*-F compound. This becomes no longer a surprise when it is realized that the σ_I -hole is
390 indeed slightly closer to the F nucleus in **7** than in **6** (5.44 and 5.70 Å, respectively), because *meta*-F
391 substitution leads to a *trans* rather than to a *cis* σ_I -S-C_{Ar}-F minimum geometrical conformation. As a
392 result, the negative V(F) contribution, counteracting the positive V(S) contribution, is lowest in
393 magnitude for the *meta*-F compound. The sum of V(F) and V(S) contributions already accounts for the
394 σ_I trend in **6-7** compounds (-0.0236 and -0.0249 au, respectively). Despite the more negative V(S+F)
395 contribution in **5** relative to **7** (-0.0416 and -0.0249 au, respectively), almost equal σ_I values occur for
396 *ortho* (**5**) and *para* (**7**) F-substitution. This arises because of a larger positive contribution of the C atom
397 linked to the fluorine (these contributions are denoted in bold in Table 6) which compensates the more
398 negative V(S+F) contribution (-0.0416 and -0.0249 au, respectively). The small changes in the V(Het)
399 values play only a minor role in defining the σ_I trend in **5-7** compounds. The SF analysis of the σ -holes
400 in **5-7** allows for an unprecedented insight on the effect of the F-substitution pattern. Minimum energy
401 geometrical conformation also plays a significant role and it cannot be ignored. If not taken into account,
402 the largest σ_I value for **6** could not find an easy explanation. The largest F distance from σ_I in the *meta*
403 substituted compound realizes the best compromise between the activation of S induced by the presence
404 of the F atom and the counteracting effect on the EP positive σ -hole due to the negative EP contribution
405 from this same atom.

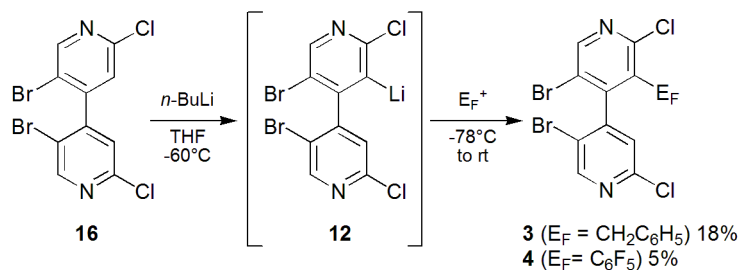
406 This kind of analysis confirmed the pivotal role of sulphur in the enantioseparation and, in this
407 perspective, the decrease of selectivity changing the 2,6-difluoro pattern of **8** (Table 5, entry 5, $\alpha = 1.18$)
408 to the 2,4-difluoro of **9** (Table 5, entry 6, $\alpha = 1.11$) could be explained on the basis of the minor

409 contribution of the carbon skeleton to σ_I induced by fluorine located at the *para* position compared to
410 *ortho* position.

411 Concerning the effect induced by the number of fluorine atoms on the aromatic ring, in the series **5**, **8**
412 and **10** (Table 5, entries 2, 5 and 7) containing 1, 2, and 3 fluorine atoms, respectively, k_1 , k_2 and α
413 increased as the number of fluorine atoms (Fig. S8) and, in particular, selectivity tended to increase
414 moderately as the max EP on σ_I and Ar_F (*o*-F (**5**, $\alpha = 1.17$; max $\text{EP}_{\sigma_I} = 69.8$ kJ/mol) < *o,o*-F₂ (**8**, $\alpha =$
415 1.18; max $\text{EP}_{\sigma_I} = 80.2$ kJ/mol; max $\text{EP}_{\text{Ar}_F} = 21.6$ kJ/mol) < *o,o,m*-F₃ (**10**, $\alpha = 1.45$; max $\text{EP}_{\sigma_I} = 92.0$
416 kJ/mol; max $\text{EP}_{\text{Ar}_F} = 48.1$ kJ/mol)). Accordingly, thermodynamic parameters derived for compound **8**
417 (Table S7) are lower ($\Delta\Delta H = -2.49$ kJ·mol⁻¹, $\Delta\Delta S = -6.96$ J·K⁻¹·mol⁻¹, $\Delta\Delta G = -0.41$ kJ·mol⁻¹) than the
418 corresponding values associated to the enantioseparation of **1** ($\Delta\Delta H = -1.96$ kJ·mol⁻¹, $\Delta\Delta S = -5.32$ J·K⁻¹·
419 mol⁻¹, $\Delta\Delta G = -0.37$ kJ·mol⁻¹), under the same elution conditions (CDMPC/mix A).

420 3.4. Impact of recognition sites generated by local electron depletion: σ -hole vs π -hole.

421 Finally, with the aim to distinguish the contribution of the chalcogen site (sulphur) from that of the
422 fluorinated π -hole, compounds **3** and **4** were designed and prepared by deprotolithiation of 2,2'-
423 dichloro-5,5'-dibromo-4,4'-bipyridine **16** [34]. Then, lithio intermediate **12** was trapped by the proper
424 electrophile (pentafluorobenzyl bromide or hexafluorobenzene), furnishing **3** and **4** (18% and 5% yields,
425 respectively) (Scheme 2). Assignment of absolute configuration for **4** was achieved by single crystal
426 XRD analysis (Supplementary data).

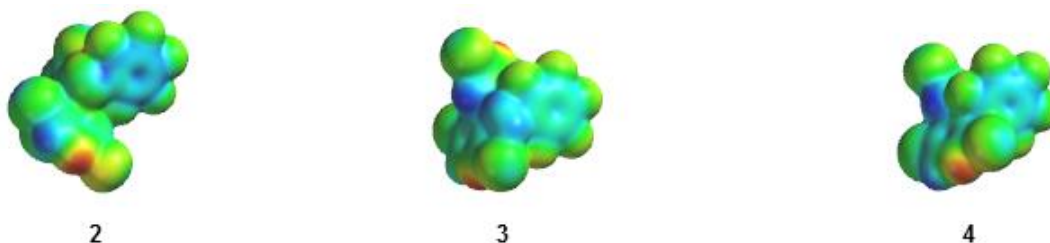


Scheme 2. Synthesis of 4,4'-bipyridines **3** and **4**.

429 The orthogonal HPLC protocol was applied to compounds **3** and **4** and the obtained chromatographic
 430 results were compared to the corresponding outcomes of **2** (Table 7).

431 The comparison between the chromatographic parameters of compound **2**, **3** and **4** (Fig. S9) proved
 432 the pivotal role of the π -hole on the perfluorinated phenyl ring as recognition site. Indeed, the following
 433 observations emerged:

434 **Table 7**
 435 Substitution pattern, retention, selectivity and max EP at the π -hole (Ar_F) of 5,5-dibromo-2,2'-dichloro-4,4'-bipyridines **2**, **3** and **4** on
 436 CDMPC and CCMPC under normal phase (NP) and polar organic (PO) elution modes (FR 0.8 ml/min, $T = 25^\circ C$).



437

CSP ^a	MP ^b	Parameter ^c	2 (-SC ₆ F ₅) 105.7 kJ/mol ^d	3 (-CH ₂ C ₆ F ₅) 89.8 kJ/mol ^d	4 (-C ₆ F ₅) 101.1 kJ/mol ^d
CDMPC	A	k_1	1.14 (<i>M</i>)	1.21	0.65 (<i>M</i>)
		k_2	6.12 (<i>P</i>)	4.39	0.97 (<i>P</i>)
		α	5.34	3.62	1.48
CCMPC	A	k_1	0.90 (<i>M</i>)	1.22	0.48 (<i>M</i>)
		k_2	1.18 (<i>P</i>)	1.80	0.51 (<i>P</i>)
		α	1.31	1.48	1.07
CDMPC	B	k_1	1.26 (<i>M</i>)	1.32	0.71 (<i>M</i>)
		k_2	4.61 (<i>P</i>)	3.68	1.10 (<i>P</i>)
		α	3.67	2.78	1.56
CDMPC	C	k_1	0.87 (<i>M</i>)	0.67	0.51 (<i>M</i>)
		k_2	1.80 (<i>P</i>)	1.36	0.67 (<i>P</i>)
		α	2.06	2.02	1.31

438 ^a CDMPC cellulose *tris*(3,5-dimethylphenylcarbamate); CCMPC cellulose *tris*(3-chloro-4-methylphenylcarbamate).

439 ^b MP, Hex/IPA 90:10 (A); Hex/IPA/MeOH 90:5:5 (B); MeOH 100% (C).

440 ^c For compounds **2** and **4**, absolute configuration of the eluted peaks is reported.

441 ^d max EP (electrostatic potential) π -hole (Ar_F).

442 i) in general, compound **4** showed lower retention and selectivity compared to **2** and **3** and a different
 443 recognition mechanism seemed to occur. From the EPS generated for **4** by calculation, it could be
 444 observed that the aromatic ring at the position 3 of the 4,4'-bipyridine scaffold is sterically hindered by
 445 the adjacent chlorine at the 2 position. This condition prevents the penetration of the analyte into the
 446 groove as proved by the low values of retention of both first and second eluted peaks ($0.48 \leq k_1 \leq 0.71$;
 447 $0.51 \leq k_2 \leq 1.10$) obtained for **4** with all four chromatographic systems. This hypothesis appeared in
 448 agreement with the positive values of $\Delta G_{298 K}$ derived for **4** in almost all cases ($0.08 \leq \Delta G_{298 K} [kJ \cdot mol^{-1}]$)

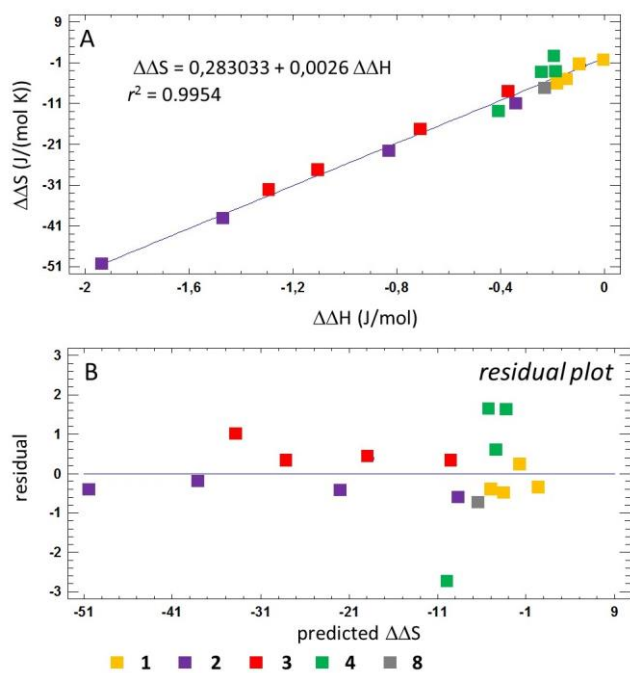
449 ≤ 1.81) (Table S8), depending on the lower value of the entropic term $T\Delta S$ ($-15.15 \leq T\Delta S$ [$\text{kJ}\cdot\text{mol}^{-1}$] $\leq -$
450 9.05) compared to the enthalpic term ΔH ($-15.07 \leq \Delta H$ [$\text{kJ}\cdot\text{mol}^{-1}$] ≤ -7.38) in the Gibbs equation ($\Delta G =$
451 $\Delta H - T\Delta S$, $\Delta H < 0$ and $T\Delta S < \Delta H$). On this basis, weak hydrophobic π - π interactions between the
452 analyte and the aromatic moieties in the outer regions of the CSP are likely to govern selectivity in this
453 case. Indeed, by introducing MeOH in the MP (*mix B*), which favours hydrophobic behaviours,
454 selectivity of **4** on CDMPC increases ($\alpha = 1.56$) compared to the selectivity obtained with *mix A* on the
455 same CSP ($\alpha = 1.48$).

456 ii) it is worth comparing the chromatographic behaviours of the couple 5,5'-dibromo-2,2'-dichloro-3-
457 phenyl-4,4'-bipyridine (**17**) / **1** (Fig. S10) and the couple **4** / **2** (Fig. S9). In both cases, the substitution
458 pattern of **17**, **4** and **1**, **2** can be correlated by introducing a sulphur atom as spacer between the
459 heteroaromatic scaffold and the phenyl ring. Interestingly, this structural variation has a dramatic effect
460 on selectivity only for **2**, which bears both σ - and π -hole ($\max EP_{\sigma I} = 114.4$ kJ/mol; $\max EP_{\text{ArF}} = 105.7$
461 kJ/mol), whereas it has no effect for **1** ($\max EP_{\sigma I} = 59.9$ kJ/mol). Indeed, the enantioseparation traces of
462 **1** and **17** are superimposable (Fig. S10);

463 iii) the EPS generated for compound **3** showed a more accessible π -hole due to the presence of a
464 methylene ($-\text{CH}_2-$) spacer between the 4,4'-bipyridine and the perfluorinated ring, even with a lower
465 depth (89.9 kJ/mol) compared to **4** (101.1 kJ/mol). For **3**, higher retention and selectivity were observed
466 compared to **4** (**3**: $k_1 = 1.21$, $k_2 = 4.39$, $\alpha = 3.62$; **4**: $k_1 = 0.65$, $k_2 = 0.97$, $\alpha = 1.48$), which are likely due
467 to the conformational flexibility induced by the methylene spacer. In particular, on CDMPC, **3** showed
468 lower values of $\Delta\Delta H$ ($-12.99 \leq \Delta\Delta H$ [$\text{kJ}\cdot\text{mol}^{-1}$] ≤ -7.11) and $\Delta\Delta S$ ($-32.81 \leq \Delta\Delta S$ [$\text{J}\cdot\text{K}^{-1}\cdot\text{mol}^{-1}$] ≤ -17.98)
469 compared to **4** ($-2.29 \leq \Delta\Delta H$ [$\text{kJ}\cdot\text{mol}^{-1}$] ≤ -1.87 ; $-4.03 \leq \Delta\Delta S$ [$\text{J}\cdot\text{K}^{-1}\cdot\text{mol}^{-1}$] ≤ -3.15). On the contrary, on
470 CCMPC higher values of $\Delta\Delta H$ and $\Delta\Delta S$ were derived for **3** (**3**: $\Delta\Delta H = -3.64$ $\text{kJ}\cdot\text{mol}^{-1}$; $\Delta\Delta S = -8.84$ $\text{J}\cdot\text{K}^{-1}$
471 $\cdot\text{mol}^{-1}$; **4**: $\Delta\Delta H = -3.94$ $\text{kJ}\cdot\text{mol}^{-1}$; $\Delta\Delta S \leq -12.68$ $\text{J}\cdot\text{K}^{-1}\cdot\text{mol}^{-1}$). These variations dependent on the CSP
472 structures appeared consistent with a mechanism controlled by a lone pair- π -hole bond, involving **3** and

473 the carbonyl lone pair in the inner part of the CSP. In this perspective, as the Lewis basicity of the
 474 carbonyl decreases in the CCMPC, consequently, enantiomer thermodynamic stabilization also
 475 decreases. On the contrary, for **4** the thermodynamic stabilization by means of π - π interactions is higher
 476 with the distinctive 3-chloro-4-methylphenyl (CCMPC) compared to the 3,5-dimethylphenyl (CDMPC),
 477 likely because of different stereoelectronic properties;

478 iv) compound **2** showed higher k_2 and selectivity than **3** on CDMPC (**2**: $k_2 = 6.12$, $\alpha = 5.34$; **3**: $k_2 =$
 479 4.39 , $\alpha = 3.62$), whereas lower retention and selectivity on CCMPC (**2**: $k_1 = 0.90$, $\alpha = 1.18$; **3**: $k_1 = 1.22$,
 480 $\alpha = 1.48$) was observed. On the contrary, the two compounds showed very similar selectivity on
 481 CDMPC with *mix C* (**2**: $\alpha = 2.06$; **3**: $\alpha = 2.02$), where pure MeOH, as MP, prevent formation of polar
 482 interactions. Taking into account that the substitution pattern of **3** and **2** could be correlated by changing
 483 the methylene spacer to sulphur at the 3-position, the critical function of sulphur on selectivity emerged.

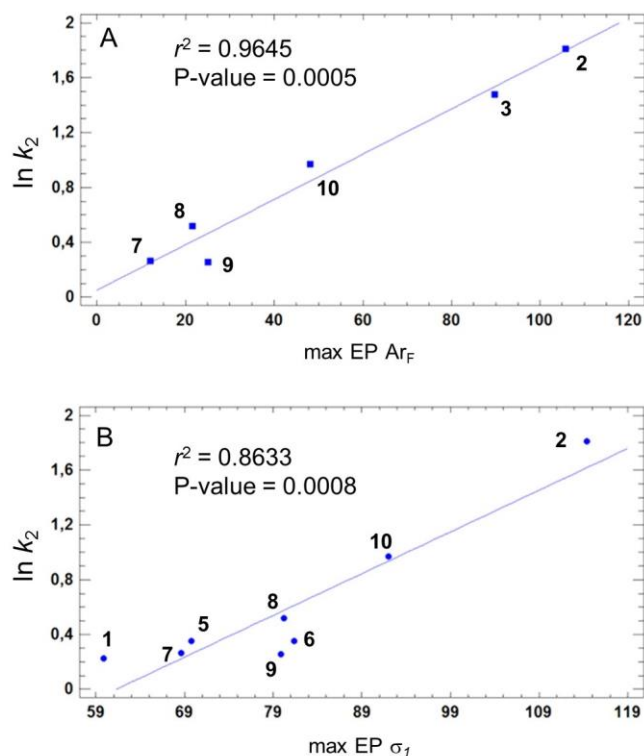


484
 485 **Fig. 5.** A. Enthalpy-entropy ($\Delta\Delta S$ vs $\Delta\Delta H$ values x 10000) compensation for compounds **1**, **2**, **3**, **4** and **8**
 486 on CDMPC and CCMPC under normal phase (NP) and polar organic (PO) elution modes (*FR* 0.8
 487 ml/min); B. Residual plot ($\Delta\Delta S$ values).
 488

489 Analysis of the collected thermodynamic parameters for **1-4** and **8** (Tables 4, S7 and S8) revealed that
 490 $\Delta\Delta H$ and $\Delta\Delta S$ change proportionally. The changes in the two quantities essentially cancel out each

491 other, resulting in only small changes in $\Delta\Delta G$. This phenomenon is known as entropy-enthalpy
492 compensation (EEC) and is illustrated graphically by the linear relationship between $\Delta\Delta H$ and $\Delta\Delta S$ (Fig.
493 5). Enthalpy-entropy compensation gave a straight line with a good correlation coefficient ($r^2= 0.9954$)
494 and no deviation from linearity was observed. This could confirm that the same type of discrimination
495 mechanism governs the examined enantioseparations with a level of efficacy dependent on the
496 substitution pattern.

497 With the aim to examine in depth the results of the EEC, the residual ($\Delta\Delta S_{\text{predicted}} - \Delta\Delta S_{\text{experimental}}$) plot
498 values (Table S9) derived from the linear regression analysis were compared. Taking the sum of the
499 residual values of **2** as reference absolute value (1.46), interestingly, in accord with the experimental
500 outcomes, the corresponding absolute values calculated for **1**, **3** and **4** showed a deviation from **2**
501 following the order **2** (1.46) < **1** (1.48) < **3** (2.0) < **4** (6.58_[A1]).



502

503 **Fig. 6.** Linear regression analysis describing the relationships between $\ln k_2$ and the max EP Ar_F (π -hole)
504 (A) and the max EP on σ_1 (B) for compound **1-3** and **5-10**.

505 Finally, the influence of the two regions of electron depletion on retention of the second eluted
506 enantiomers was verified by simple linear regression using $\ln k_2$ and max EPs on Ar_F (π -hole) and σ_1 as
507 dependent and independent variables, respectively. On the basis of the described chromatographic
508 behaviour, compound **4** was excluded from the analysis. For compounds **2**, **3** and **7-10**, which are
509 characterized by positive values of EPs on Ar_F, the result of fitting a simple linear regression model to
510 describe the relationship between $\ln k_2$ and max EPs on Ar_F is reported in Fig. 6A ($r^2= 0.9645$). In this
511 case, the P-value of the considered independent variable, max EPs on Ar_F, is 0.0005 indicating a
512 statistically significant relationship (P-value > 0.05).

513 Then, for compounds **1**, **2** and **5-10**, the correlation between $\ln k_2$ and the max EPs on σ_1 is reported
514 in Fig. 7B ($r^2= 0.8633$). The P-value of the considered independent variable, the max EPs on σ_1 , is low
515 (0.0008), showing again a statistical significant relationship (P-value < 0.05) between selectivity and the
516 electron depletion on sulphur.

517 On the basis of experimental results, theoretical data and statistical evaluations, it is reasonable to
518 conclude that both σ - and π -hole bond concur to the enantioseparation outcomes of **2**. The study of
519 structurally similar compounds showed that the strength of each interaction strictly depends on analyte
520 and CSP structures and MP polarity. In this regard, it is interesting to mention that several recent articles
521 reported on the interplay between σ -hole and π -hole bonds [38].

522 *3.5. Molecular dynamics.*

523 MD calculations were performed to simulate the interaction modes of compound **2** with the CDMPC.
524 A massless dummy atom (MA_D) connected to sulphur was introduced manually in **2**, by using distance
525 (1.6 Å) and charge (0.2 units of positive charge) fixed arbitrarily (see Supplementary data for details).
526 On this basis, with the aim to compare qualitatively the MD outcomes under different molecular
527 situations, the calculations were performed with and without the MA_D, and Hex solvent effects were
528 taken into account in accord with the method used in the HPLC screening.

529 The MD protocol proposed herein may not lead to the selector-selectand complexes with the global
530 minimum energy, however some interesting behaviour could be observed, which confirmed the pivotal
531 role of sulphur as a chalcogen recognition site in **2**:

532 i) by carrying out 10 ns MD, the trajectory plots for CDMPC and **2** showed stable interactions when
533 the MA_D correction was applied, with narrow fluctuations over 10 ns compared to the larger fluctuations
534 observed when MA_D correction was not applied (Fig. S30);

535 ii) in all simulations performed by using the MA_D correction, contacts between sulphur and the
536 carbonyl groups of the carbamate moieties of the CSP were observed. Taking into account that the MA_D
537 correction was introduced arbitrarily, a measure of the geometrical parameters of the contact was not
538 performed;

539 iii) finally, the occupancy graphs generated from the MD trajectories for the complexes CDMPC /
540 (*M*)-**2** (with MA_D), CDMPC / (*P*)-**2** (with MA_D), and CDMPC / (*P*)-**2** (without MA_D) were compared
541 (Fig. S31). The occupancy analysis allowed to evaluate which regions of space were highly populated by
542 the analysis over 10 ns MD. Interestingly, by using the MA_D, the first eluted enantiomer (*M*)-**2** showed
543 occupancy volumes in the outer region of the CSP, whereas for the second eluted enantiomer (*P*)-**2**
544 occupancy volumes were also generated in the inner regions of the polymer. On the contrary, not
545 applying the MA_D correction, for the enantiomer (*P*)-**2** the occupancy volumes were shown to move
546 toward the outer regions of the polymer.

547 **4. Conclusions**

548 The enantioselectability of fluorinated 3-(aryl)thio-4,4'-bipyridines on CDMPC was shown to
549 increase as the EP related to regions of local electron depletion on the analyte becomes increasingly
550 positive. This observation represents the core of our study which, on the basis of theoretical data and
551 experimental results, furnishes evidences that stereoselective chalcogen and π -hole bonds, so far
552 unexplored in HPLC environment, can drive enantioseparations. A new approach, based on the

553 extension of the Source Function tool to the EP and enabling to get insights on the chemical origin of
554 these enantioseparation “drivers”, has for the first time been proposed.

555 Computational evaluation of molecular properties allowed to design analytes suitable as probes and,
556 in parallel, to clarify some aspects of the observed chromatographic behaviours. Finally, the introduction
557 of a massless dummy ligand, positively charged to mimic the electron depletion on sulphur, allowed to
558 explore the dynamic behaviour of the enantiomers of **2** on CDMPC, obtaining theoretical results
559 qualitatively in accord with the experimental outcomes.

560 On this basis, enantioseparations of atropisomeric test probes containing heavier chalcogen atoms are
561 currently under investigations.

562 **Acknowledgements**

563 This work has been supported by Università Ca' Foscari di Venezia, Italy (Dipartimento di Scienze
564 Molecolari e Nanosistemi, DSMN ADIR funds). The Service Commun de Diffraction des rayons X-
565 Université de Lorraine is thanked for providing access to crystallographic facilities. We thank the
566 International Center Frontier Research in Chemistry (icFRC) and the Laboratory of Excellence for
567 Complex System Chemistry (LabEx CSC).

568 **Appendix A. Supplementary data**

569 Supplementary data associated with this article can be found, in the online version, at doi:

570 **References**

- 571 [1] G.K.E. Scriba, Chiral recognition in separation science - an update, *J. Chromatogr. A* 1467 (2016)
572 56-78.
- 573 [2] H. Lorenz, A. Seidel-Morgenstern, Processes to separate enantiomers, *Angew. Chem. Int. Ed.* 53
574 (2014) 1218-1250.
- 575 [3] J.C. Lang, D.W. Armstrong, Chiral surfaces: the many faces of chiral recognition, *Current Opinion*
576 *in Colloid & Interface Science* 32 (2017) 94-107.

- 577 [4] H.-J. Schneider, Binding mechanisms in supramolecular complexes, *Angew. Chem. Int. Ed.* 48
578 (2009) 3924 – 3977.
- 579 [5] M. Lämmerhofer, Chiral recognition by enantioselective liquid chromatography: mechanisms and
580 modern chiral stationary phases, *J. Chromatogr. A* 1217 (2010) 814-856.
- 581 [6] A. Bauzá, T.J. Mooibroek, A. Frontera, The bright future of unconventional σ/π -hole interactions,
582 *ChemPhysChem* 16 (2015) 2496-2517.
- 583 [7] L. Brammer, Halogen bonding, chalcogen bonding, pnictogen bonding, tetrel bonding: origins,
584 current status and discussion, *Faraday Discuss.* 203 (2017) 485-507.
- 585 [8] P. Politzer, J.S. Murray, T. Clark, Halogen bonding and other σ -hole interactions: a perspective,
586 *Phys. Chem. Chem. Phys.* 15 (2013) 11178-11588.
- 587 [9] P. Peluso, V. Mamane, S. Cossu, Liquid chromatography enantioseparations of halogenated
588 compounds on polysaccharide-based chiral stationary phases: role of halogen substituents in
589 molecular recognition, *Chirality* 27 (2015) 667–684.
- 590 [10] P. Peluso, V. Mamane, E. Aubert, S. Cossu, Insights into the impact of shape and electronic
591 properties on the enantioseparation of polyhalogenated 4,4'-bipyridines on polysaccharide-type
592 selectors. Evidence for stereoselective halogen bonding interactions, *J. Chromatogr. A* 1345
593 (2014) 182–192.
- 594 [11] P. Peluso, V. Mamane, E. Aubert, A. Dessì, R. Dallochio, A. Dore, P. Pale, S. Cossu, Insights
595 into halogen bond driven enantioseparations, *J. Chromatogr. A* 1467 (2016) 228–238.
- 596 [12] B. Chankvetadze, Recent developments on polysaccharide-based chiral stationary phases for
597 liquid-phase separation of enantiomers, *J. Chromatogr. A* 1269 (2012) 26–51.
- 598 [13] P. Peluso, V. Mamane, R. Dallochio, A. Dessì, R. Villano, D. Sanna, E. Aubert, P. Pale, S.
599 Cossu, Polysaccharide-based chiral stationary phases as halogen bond acceptors: A novel strategy

- 600 for detection of stereoselective σ -hole bonds in solution, *J. Sep. Sci.* 6 (2018), DOI:
601 10.1002/jssc.201701206.
- 602 [14] K.T. Mahmudov, M.N. Kopylovich, M.F.C. Guedes da Silva, A. J. L. Pombeiro, Chalcogen
603 bonding in synthesis, catalysis and design of materials, *Dalton Trans.* 46 (2017) 10121–10138.
- 604 [15] P.C. Ho, P. Szydlowski, J. Sinclair, P.J.W. Elder, J. Kübel, C. Gendy, L. Myongwon Lee, H.
605 Jenkins, J.F. Britten, D.R. Morim, I. Vargas-Baca, Supramolecular macrocycles reversibly
606 assembled by Te...O chalcogen bonding, *Nat. Commun.* 7:11299 (2016) doi:
607 10.1038/ncomms11299.
- 608 [16] S. Benz, M. Macchione, Q. Verolet, J. Mareda, N. Sakai, S. Matile, Anion transport with
609 chalcogen bonds, *J. Am. Chem. Soc.* 138 (2016) 9093–9096.
- 610 [17] J.Y.C. Lim, I. Marques, A.L. Thompson, K.E. Christensen, V. Félix, P.D. Beer, Chalcogen
611 bonding macrocycles and [2]rotaxanes for anion recognition, *J. Am. Chem. Soc.* 139 (2017)
612 3122–3133.
- 613 [18] S. Benz, J. López-Andarias, J. Mareda, N. Sakai, S. Matile, Catalysis with chalcogen bonds,
614 *Angew. Chem. Int. Ed.* 56 (2017) 812–815.
- 615 [19] P. Wonner, L. Vogel, F. Kniep, S.M. Huber, Catalytic carbon-chlorine bond activation by
616 selenium-based chalcogen bond donors, *Chem. Eur. J.* 23 (2017) 16972–16975.
- 617 [20] A. Bauzá, T.J. Mooibroek, A. Frontera, Towards design strategies for anion– π interactions in
618 crystal engineering, *CrystEngComm* 18 (2016) 10-23.
- 619 [21] P. Peluso, S. Cossu, Comparative HPLC enantioseparation of thirty six aromatic compounds on
620 four columns of the Lux® series. Impact of substituents, shapes and electronic properties,
621 *Chirality* 25 (2013) 709-718.
- 622 [22] R.F.W. Bader, *Atoms in molecules: a quantum theory*, International Series of Monographs on
623 Chemistry 22, Oxford University Press, Oxford (1990).

- 624 [23] C. Gatti, F. Cargnoni, L. Bertini, Chemical information from the source function, *J. Comput.*
625 *Chem.* 24 (2003) 422-436.
- 626 [24] C. Gatti, The source function descriptor as a tool to extract chemical information from theoretical
627 and experimental electron densities, *Struct. Bond* 147 (2012), 193–286.
- 628 [25] A. Volkov, P. Macchi, L.J. Farrugia, C. Gatti, P.R. Mallinson, T. Richter, T. Koritsanszky,
629 XD2006 - a computer program for multipole refinement, topological analysis and evaluation of
630 intermolecular energies from experimental and theoretical structure factors (2006).
- 631 [26] C. Gatti, SF-ESI codes, Milano, Italy (2018).
- 632 [27] H. Koller, K.–E. Rimböck, A. Mannschreck, High-pressure liquid chromatography on
633 triacetylcellulose: characterization of a sorbent for the separation of enantiomers, *J. Chromatogr. A*
634 282 (1983) 89-94.
- 635 [28] Y. Shao, L.F. Molnar, Y. Jung, J. Kussmann, C. Ochsenfeld, S.T. Brown, A.T.B. Gilbert, L.V.
636 Slipchenko, S.V. Levchenko, D.P. O’Neil, R.A. Di Stasio Jr, R.C. Lochan, T. Wang, G.J.O. Beran,
637 N.A. Besley, J.M. Herbert, C.Y. Lin, T. Van Voorhis, S.H Chien, A. Sodt, R.P. Steele, V.A.
638 Rassolov, P.E. Maslen, P.P. Korambath, R.D. Adamson, B. Austin, J. Baker, E.F.C. Byrd, H.
639 Dachsel, R.J. Doerksen, A. Dreuw, B.D. Dunietz, A.D. Dutoi, T.R. Furlani, S.R. Gwaltney, A.
640 Heyden, S. Hirata, C-P. Hsu, G. Kedziora, R.Z. Khalliulin, P. Klunzinger, A.M. Lee, M.S. Lee,
641 W.Z. Liang, I. Lotan, N. Nair, B. Peters, E.I. Proynov, P.A. Pieniazek, Y.M. Rhee, J. Ritchie, E.
642 Rosta, C.D. Sherrill, A.C. Simmonett, J.E. Subotnik, H.L. Woodcock III, W. Zhang, A.T. Bell,
643 A.K. Chakraborty, D. M. Chipman, F.J. Keil, A. Warshel, W.J. Hehre, H.F. Schaefer, J. Kong, A.I.
644 Krylov, P.M.W. Gill, M. Head-Gordon, Advances in methods and algorithms in a modern
645 quantum chemistry program package, *Phys. Chem. Chem. Phys.* 8 (2006) 3172-3191.
- 646 [29] T. Lu, F. Chen, Multiwfn: A Multifunctional Wavefunction Analyzer, *J.Comp. Chem.* 33 (2012)
647 580-592.

- 648 [30] T. Lu, F. Chen, Quantitative analysis of molecular surface based on improved Marching
649 Tetrahedra algorithm, *J. Mol. Graph. Model.* 38 (2012) 314-323.
- 650 [31] K.E. Riley, K.-A. Tran, P. Lane, J.S. Murray, P. Politzer, Comparative analysis of electrostatic
651 potential maxima and minima on molecular surfaces, as determined by three methods and a variety
652 of basis sets, *J. Comput. Sci.* 17 (2016) 273-284.
- 653 [32] S. Scheiner, Comparison of various means of evaluating molecular electrostatic potentials for
654 noncovalent interactions, *J. Comput. Chem.* 39 (2018) 500-510.
- 655 [33] R.F.W. Bader, C. Gatti, A Green's function for the density, *Chem. Phys. Lett.* 287 (1998) 233-238.
- 656 [34] V. Mamane, E. Aubert, P. Peluso, S. Cossu, Lithiation of prochiral 2,2'-dichloro-5,5'-dibromo-
657 4,4'-bipyridine as a tool for the synthesis of chiral polyhalogenated 4,4'-bipyridines, *J. Org. Chem.*
658 78 (2013) 7683-7689.
- 659 [35] T. Ikai, Y. Okamoto, Structure control of polysaccharide derivatives for efficient separation of
660 enantiomers by chromatography, *Chem. Rev.* 109 (2009) 6077-6101.
- 661 [36] Kasat R. B., Wang N. -H. L., Franses E. I., Effects of backbone and side chain on the molecular
662 environments of chiral cavities in polysaccharide-based biopolymers, *Biomacromolecules* 8 (2007)
663 1676-1685.
- 664 [37] P. Peluso, V. Mamane, E. Aubert, S. Cossu, High performance liquid chromatography
665 enantioseparation of atropisomeric 4,4'-bipyridines on polysaccharide-type chiral stationary
666 phases: impact of substituents and electronic properties, *J. Chromatogr. A* 1251 (2012) 91-100.
- 667 [38] H. Wang, W. Wang, W. J. Jin, σ -Hole bond vs π -hole bond: a comparison based on halogen bond,
668 *Chem. Rev.* 116 (2016) 5072-5104.

669 **FIGURE CAPTIONS**

670 **Fig. 1.** Description of halogen bond (XB) (A) and polysaccharide-based polymers as XB acceptors (B).

671 **Fig. 2.** General description of chalcogen (ChB) (A) and π -hole bond (B).

672 **Fig. 3.** Structures of the 5,5'-dibromo-2,2-dichloro-3-substituted-4,4'-bipyridines **1-10**.

673 **Fig. 4.** Design of potential 4,4'-bipyridine-based ChBDs.

674 **Fig. 5.** A. Enthalpy-entropy ($\Delta\Delta S$ vs $\Delta\Delta H$ values x 10000) compensation for compounds **1**, **2**, **3**, **4** and **8**
675 on CDMPC and CCMPC under normal phase (NP) and polar organic (PO) elution modes (FR 0.8
676 ml/min); B. Residual plot ($\Delta\Delta S$ values).

677 **Fig. 6.** Linear regression analysis describing the relationships between $\ln k_2$ and the max EP Ar_F (π -hole)
678 (A) and the max EP on σ_1 (B) for compound **1-3** and **5-10**.

679 **Scheme 1.** Synthesis of 4,4'-bipyridines **1** and **2**.

680 **Scheme 2.** Synthesis of 4,4'-bipyridines **3** and **4**.